Chemical Engineering Journal 158 (2010) 431–440

Contents lists available at ScienceDirect

Chemical Engineering Journal

journal homepage: www.elsevier.com/locate/cej

Computational fluid dynamics simulation of a transpiring wall reactor for supercritical water oxidation

María Dolores Bermejo[a,*], Ángel Martín[a,b], Joao P.S. Queiroz[a], Iván Bielsa[a], Vicente Ríos[a], María José Cocero[a]

[a] High Pressure Process Group, Department of Chemical Engineering and Environmental Technology, Universidad de Valladolid (Spain), Prado de la Magdalena s/n, 47011 Valladolid, Spain
[b] Lehrstuhl für Verfahrenstechnische Transportprozesse, Ruhr Universität Bochum, Universitätsstraße 150, 44801 Bochum, Germany

ARTICLE INFO

Article history:
Received 19 August 2009
Received in revised form
28 December 2009
Accepted 7 January 2010

Keywords:
Supercritical water oxidation SCWO
CFD model
Transpiring wall reactor
Energy
Mass and momentum conservation equations
k–ε turbulence model
Peng–Robinson Equation of State
Heat capacity

ABSTRACT

A computational fluid dynamic (CFD) model of a transpiring wall reactor for supercritical water oxidation has been implemented and solved using the commercial software Fluent 6.3. Model results have been validated by comparison with experimental temperature profiles, and the influence of model simplifications on the accuracy of the results has been discussed. It has been found that the model presents some inaccuracies in the calculation of the maximum reaction temperature, which have been attributed to the simplifications in the calculation of thermal properties of the fluids imposed by limitations of the software. The effect of different process parameters has been studied, including transpiring water flow ratio, transpiring water temperature, flow rate and composition of the oxidant (pure oxygen or air) on different indicators of reactor performance such as temperature and composition contours, flow path lines and effluent compositions. The behaviour of three different transpiring wall designs comprising different sections of porous and non-porous materials has also been investigated. It has been found that making the upper cup of the reactor of a porous material has a very little influence on reactor performance, and therefore it is preferable to build this part of the reaction chamber using a non-porous, more durable material. On the other hand, the maximum reaction temperature in the reaction chamber can be increased if the upper part of the reaction chamber is made with a non-porous material, which is favourable for treating diluted feeds. Model results complement previous information obtained by experiments and by simplified models.

1. Introduction

The polarity of water changes with temperature and pressure. At supercritical conditions (T > 647 K, P > 22.1 MPa) water is a non-polar solvent which is able to dissolve organic compounds in any proportion. Permanent gases and particularly oxygen are also completely miscible with supercritical water. Therefore, in supercritical water the oxidation of organics can be carried out without any limitation due to interfacial transport. Waste treatment by supercritical water oxidation (SCWO) is based on this peculiar property of supercritical water. It has been demonstrated that SCWO can destroy organic wastes achieving very high efficiencies (>99%) even with very short reaction times (<1 s) [1,2].

Other physical properties of supercritical water are less favourable for the technical development of SCWO processes. Because supercritical water is a non-polar solvent, salts that are soluble in atmospheric conditions become insoluble in the supercritical region. Precipitation of these salts can cause severe problems of corrosion and clogging. Moreover, the strong oxidizing conditions in SCWO media can damage reactor construction materials. The development of new reactor designs built with appropriate materials in order to overcome these limitations is a challenging and active field of research and development [1–4].

Some of the most successful SCWO reactor designs for treatment of liquid feeds are based on the concept of the double shell [5–9]: an internal reaction chamber is built with a corrosion-resistant material capable of withstanding the high temperature and corrosive SCWO media. This reaction chamber is placed inside a high-pressure vessel, which can be built with a cheaper, less corrosion-resistant material, because this pressure vessel is not in contact with the reaction mixture. Among these double shell reactors are the transpiring wall reactors. In the transpiring wall reactor (TWR), the reaction chamber is built with a porous material. Clean cold water circulates through the pores, cooling the wall down and preventing the deposition of salts on it. In recent years, several TWR designs have been developed, with different technical

* Corresponding author. Tel.: +34 983423166.
E-mail address: mdbermejo@gmail.com (M.D. Bermejo).

1385-8947/$ – see front matter © 2010 Elsevier B.V. All rights reserved.
doi:10.1016/j.cej.2010.01.013

solutions for reagent preheating, cooling and flow control though the wall [10–13]. The High Pressure Process Group at the University of Valladolid has developed a TWR at pilot plant scale. As it will be described with more detail in Section 2, some of the distinctive features of this reactor compared to other TWR are the relatively large feed flows that it can process (up to 200 kg/h), and its mechanical design, which has only one flanged connection in one of the sides, making easier to open and close the reactor, and is prepared to hold the reactor in a vertical position, which is favourable for removing salts in a sub-critical, liquid effluent. Extensive experimentation with this reactor has been made [13] obtaining total organic carbon (TOC) removals higher than 99.9% (TOC effluent lower than 10 ppm) even working with real wastewaters [14].

In most cases, the information that can be obtained from experiments with TWR under real operating conditions is limited to temperature measurements inside the reactor and effluent characterization, because the aggressive oxidizing conditions inside the reactor make it difficult to obtain other measurements. Thus, the development of theoretical models of the process is of great interest as it provides a complement to the experimental information concerning those variables that are difficult to measure.

Several authors have developed mathematical models of SCWO reactors and particularly of TW reactors [11,12,15]. In our group, we have developed models based on the resolution of energy and mass transport balances with simple flow patterns [16]. With these models, it was possible to reproduce experimental axial temperature profiles inside the reactor as well as TOC elimination efficiencies. However, these models are not able to provide any information about radial temperature profiles, or about complex fluid dynamic processes near the transpiring wall which are important for the design and development of TW reactors. In order to obtain this information, a more complex model including the momentum balance is required.

Computational fluid dynamic (CFD) techniques have been applied by several authors to obtain detailed information about velocity and temperature profiles in SCWO reactors and hydrothermal flames. Oh et al. [17] developed a CFD model of a MODAR SCWO reactor. Zhou et al. [18] incorporated the SUPERTRAPP code for thermodynamic and transport properties of hydrocarbon mixtures into a CFD simulation. Moussière et al. [19] presented a CFD model of SCWO in a tubular reactor, including a detailed discussion about the selection of the model used to represent reaction kinetics. Two different models were tested, an Arrhenius law and the Eddy Dissipation Concept (EDC), and authors concluded that results obtained with both models were in general agreement with experimental data, but the EDC model performed better in the prediction of hot spots in the reaction wall. Sierra-Pallares et al. [20] also succeeded in the application of CFD with the modified multiple-timescale EDC-MTS reaction kinetics to describe the oxidation of methanol in a hydrothermal flame, predicting the experimental temperature of the flame with a deviation lower than 10%. Narayanan et al. [21] presented a CFD model of a hydrothermal flame, using the EDC approach to model reaction kinetics and the Peng–Robinson Equation of State to model fluid properties. The model was used to provide valuable information for the construction of a new reactor, including an analysis of the influence of the location of temperature probes. A detailed revision about the subject can be found elsewhere [22].

The aim of this work is to develop a CFD model of the TWR built and tested in the University of Valladolid, in order to obtain detailed information about radial temperature profiles and fluid dynamics near the transpiring wall that complements experimental results. Special attention is paid to the selection of suitable models for the calculation of reaction mixture physical properties. The model is then used to analyse the differences in the performance of the TWR designs tested in the University of the Valladolid, as well as the scale-up of the design for operation on a larger scale demonstration plant [5].

2. Experimental set-up

A schematic diagram of the TWR of the University of Valladolid is presented in Fig. 1. The reactor has an internal volume of 10 L and a height of 1.5 m. The pressure shell is made of stainless steel with an inner diameter of 90 mm, and the transpiring wall is a porous Ni-alloy tube with an inner diameter of 74 mm. The reactor is placed in vertical position inside a safety U-shaped concrete wall. Wastewater and air or oxygen inlets are located at the bottom of the reactor. Inside the reactor the two streams are brought into contact with a static mixer. The mixer outlet is located in the upper part of the reaction chamber. Inside the reactor chamber, the oxidation reaction is completed and products are mixed and cooled down with the transpiring water flow, before leaving through the outlets located at the bottom of the reactor.

Three different transpiring wall designs have been tested with this reactor. They are also shown in Fig. 1. In the first one, the whole wall is constructed with porous Ni-alloy metal sheets. In the second one, the upper cap of the wall is not porous. In the third one, only the middle section of the wall is porous. More details about the transpiring wall designs were given in a previous work [13].

The reactor has been operated in two different pilot plants. The first one is located on the premises of the University of Valladolid, and it has a maximum treatment capacity of 40 kg/h of wastewater using air as oxidant. The second one is located on the site of a waste treatment factory and it has a maximum capacity of 200 kg/h of waste using pure oxygen as the oxidant. Both plants have been used to treat synthetic wastes using 2-propanol (technical grade 2-propanol with a purity of 99% supplied by Cofarcas, Spain) as the model organic compound as well as real wastes. More details about the pilot plants were given in previous works [5,13].

3. Model description

The mathematical model is constituted by the conservation equations of mass, energy and momentum which were solved together with a realizable k–ε model for turbulent flow and standard wall functions [20,23]. Implementation and resolution of these conservation equations were done with the commercial software Fluent 6.3.

3.1. Model assumptions and simplifications

Conservation equations were solved considering 2D axisymmetric coordinates. This simplification makes it impossible to implement the real location of the reactor outlets in the simulation geometry. Therefore, as a simplification, it has been considered that the whole lowest transversal section of the reactor is an outlet. However, the rest of the elements of the reactor can be correctly described with 2D coordinates. The incorrect location of the reactor outlets can be expected to have a minimal impact on simulation results near the mixer outlet in the upper section of the reaction chamber, which is the most important region of the reactor with respect to the analysis of the behaviour of the transpiring wall. On the other hand, using 2D coordinates instead of 3D reduces model complexity as well as the required computational effort.

In most experiments, the inlet temperature of air and reagents is below the critical point and therefore a biphasic gas–liquid mixture is formed inside the static mixer, which only becomes a single phase once that temperature increases due to the heat of reaction. A rigorous model of the mixing process in the static mixer and of

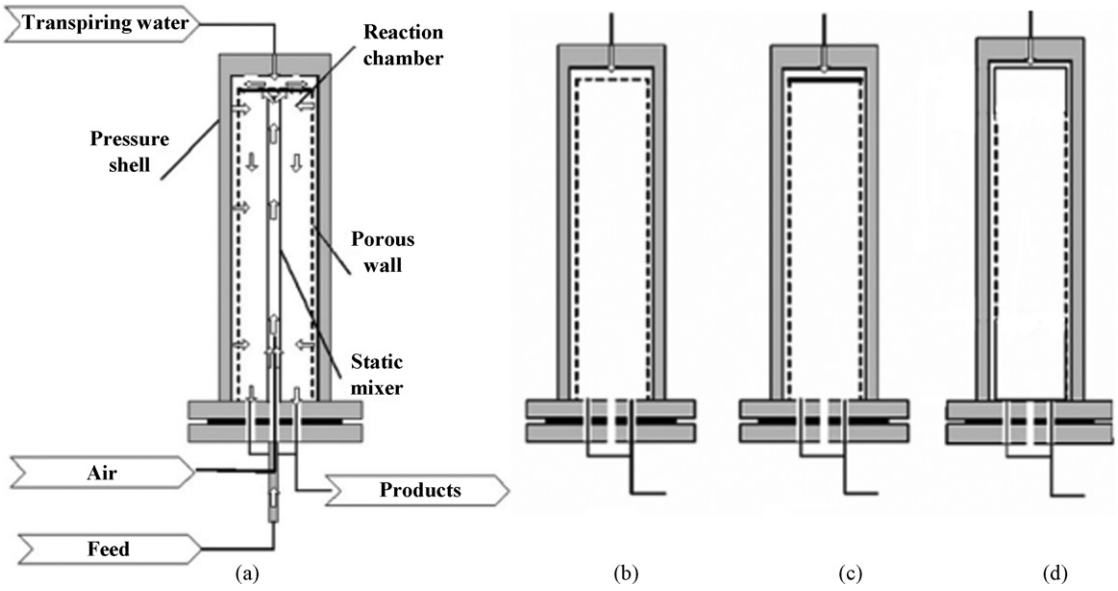

Fig. 1. (a) Scheme of the TWR. Designs of transpiring walls: (b) design 1, the whole wall is made of porous metal. (c) Design 2, the cylindrical element is made of porous metal while the cap is made of non-porous metal. (d) Design 3: only the central section of the cylindrical element is made of porous metal.

the transition from a biphasic to a single phase flow would be very complex. Because the main aim of this work is to investigate radial profiles in the reaction chamber and near the transpiring wall, as a simplification the existence of a two-phase flow inside the static mixer has been neglected, and instead it has been assumed that the feed and the oxidant are perfectly mixed from the beginning of the static mixer. It is then expected that in the model the oxidation reaction will begin earlier in the static mixer than in the actual experiments. The residence time in the static mixer is short, and the inner volume of the static mixer is 0.02 L, compared to 6.5 L in the reaction chamber. Therefore the reaction progress inside the mixer is also low (as it will be show in Section 4), this simplification has a little influence on the prediction of temperature and composition profiles inside the reaction chamber.

In all simulations, the feed was a synthetic waste containing a certain amount of 2-propanol. This considerably simplifies the calculation of physical properties with respect to real waste.

In addition to these assumptions, some simplifications had to be done in the calculation of transport and thermodynamic properties due to the limitations of the Fluent 6.3 code in this respect, as described later in Sections 3.4 and 3.5.

3.2. Meshing

Model geometry definition and meshing was performed using the commercial software Gambit. The calculation mesh consists of 65,000 cells. Preliminary simulations were performed to ensure that with this number of cells simulation results were independent of mesh size.

3.3. Kinetic model

A simplified kinetic model was used which consists of two reaction paths: the direct oxidation of the organic matter to carbon dioxide and water, and the slower oxidation through the formation of a recalcitrant reaction intermediate, in this case acetic acid. The reaction constants were obtained from the work of Li et al. [24]. In previous works, it has been demonstrated that this kinetic model is suitable for describing SCWO process [5,16,25]. The kinetic scheme is shown in the Supplementary Material (Fig. S1).

Because as a simplification it has been considered that reagents and oxidant are completely mixed since the beginning of the static mixer (as described in Section 3.2), the use of a kinetic model for the characterization of micromixing such as the eddy dissipation model [19–21] is not justified. Therefore reaction kinetics has been calculated using the finite-rate Arrhenius equations.

3.4. Transport properties

Molecular viscosities and conductivities of the pure compounds were obtained from the NIST database [26]. The corresponding properties of the fluid mixture were calculated as the mass fraction average of pure component properties:

$$\bar{Y} = \sum_{i}^{nc} x_i Y_i \quad (1)$$

3.5. Thermodynamic properties

Fluid mixture density was calculated with the Peng–Robinson Equation of State (PR-EoS) with the Magoulas–Tassios translated volume correction [27]. Because the resolution of the model is very computationally intensive and involves the evaluation of density in every cell of the mesh at each iteration step, only simple EoS models which require short and fast calculations are recommendable. It has been previously shown that the translated volume PR-EoS can calculate SCWO fluid densities with reasonable accuracy [28]. The PR-EoS was implemented using a Fluent User Defined Function (UDF).

Unfortunately, the implementation of a constitutive equation for the calculation of thermal properties through an UDF is not possible in Fluent 6.3. This software only allows defining the heat capacity C_p of the pure components as a function of temperature. The heat capacity of the reaction mixture is then calculated as a mass average as shown in Eq. (1). In a previous work [28] it has been shown that with this approach a peak in the heat capacity of the fluid mixture is obtained near the critical point of water due to the peak in the heat capacity of pure water in that temperature range. Because the real heat capacity of the fluid mixture

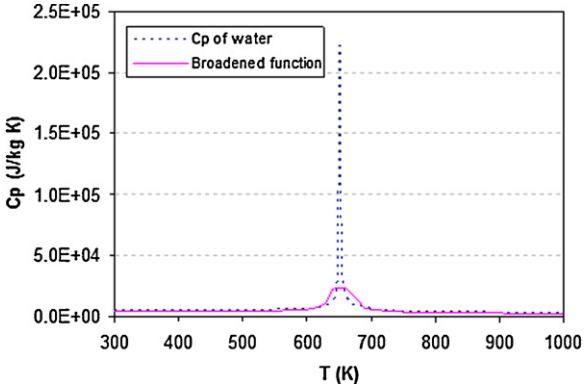

Fig. 2. Real and broadened C_p functions of pure water.

does not have this peak, it is expected that with this approach calculated temperatures will be lower than experimental temperatures.

The definition of fluid thermal properties as a table of heat capacity vs. temperature of limited size poses an additional difficulty: because the heat capacity of water varies sharply near its critical point, the entries of the table have to be selected very carefully in order to ensure that they correctly describe the peak of C_p and that the integration of the C_p yields the correct value of enthalpy. Moreover, it has been observed that Fluent incorrectly integrates the table of C_p when the difference in temperatures between adjacent table entries is too small (<1 K) or when the slope of C_p vs. T is too high, yielding simulation results that do not fulfil the global energy balance. To circumvent this limitation, an "apparent" water C_p vs. T table has been defined. In this table, the C_p peak has been broadened and its slope has been made less pronounced with respect to the real behaviour of the heat capacity of water in order to avoid inaccurate integration by Fluent. Fig. 2 presents a comparison of the real and broadened water C_p functions. Care has been taken to ensure that the area of the broadened peak is equal to the area of the real peak. This ensures that the integration of the C_p function yields the correct value of enthalpy. In this figure it can be seen that only small errors can be expected in the region around the critical point of water. Therefore, this approach will have a negligible in the final results, except in sections of the reactor where temperature is close to the critical point of water, which as will be shown in Section 4 only occurs with some process conditions at the inlet of the static mixer or at the outlet of the reactor. The same limitation and the same solution were found by other authors working on CFD simulations of SCWO reactors with Fluent [29]. The table of water C_p vs. T used in simulations is provided with this article as Supplementary Material (Table S1). A figure presenting a comparison between the real enthalpy of water and the calculations with the broadened profile, which demonstrates that the broadened C_p function yields correct values of enthalpy, is also provided in the Supplementary Material (Fig. S2).

4. Results and discussion

4.1. Comparison with experimental results

Fig. 3(a) shows a comparison between experimental and calculated temperature profiles in the reactor. These profiles correspond to an experiment performed with the 3rd design of the transpiring wall (shown in Fig. 1) and with the following process conditions: a feed flow of 22 kg/h with an isopropanol concentration of 8 wt% and an inlet temperature of 633 K, with 19.2 kg/h of air as oxidant and a transpiring water flow of 15.1 kg/h entering the reactor at 298 K. It can be seen that the CFD model underpredicts the maximum reaction temperature experimentally observed in the upper part of the reaction chamber: The maximum temperature calculated with the model is 830 K, and the maximum temperature observed in experiments is 950 K. Fig. 3(b) and (c) shows comparisons of experimental and calculated profiles obtained with the simple flow pattern model [16]. In Fig. 3(b) the heat capacity of the fluid mixture has been calculated with the Peng–Robinson Equation of State, and in Fig. 3(c) it has been calculated as a mass-averaged heat capacity (Eq. (1)). It can be observed that the simple flow pattern model with PR overpredicts the maximum temperature, and that the model with mass-averaged heat capacity underpredicts the maximum temperature. The maximum temperature calculated with the simple flow pattern model and mass-averaged heat capacity is 900 K. It can be seen that the inaccuracy due to the calculation of the heat capacity as a mass-average results in an underprediction of the maximum reaction temperature in the simple flow pattern model as well as in the CFD model, as it may be expected by comparing the heat capacity obtained by mass average with the real heat capacity of the fluid mixture [28]. In addition to this, some inaccuracy in the results can be attributed to the simplifications introduced in the model regarding the fluid mechanics in the static mixer and the reaction kinetics (Section 3). In the simulations it has been assumed that reagents are perfectly mixed when they enter into the reactor and therefore reaction starts immediately. But in reality the reaction does not start right at the beginning of the static mixer because certain length of the mixer is required for contacting the wastewater and the oxidant streams. Moreover, it is possible that a radical reaction takes place once that a sufficient temperature is achieved, with faster kinetics than those described by the mechanism used in this work [30]. Locally faster reaction kinetics could produce higher temperatures due to reduced possibilities for heat dissipation.

In Fig. 3(a) it can be seen that the results of the CFD model regarding the outlet temperature agree well with experimental results: the experimental value is 600 K, and the calculated value is 650 K. Heat dissipation to the environment has not been considered in the CFD model, and this simplification can have contributed to the

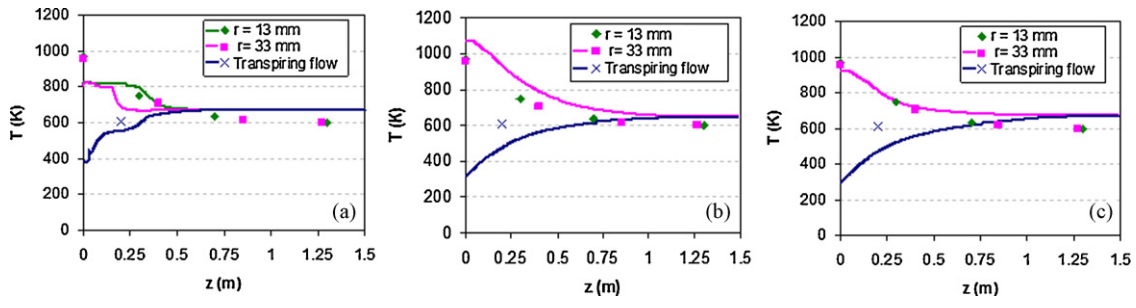

Fig. 3. Comparison of experimental and calculated temperature profiles, (a) CFD model, (b) simple flow model with Peng–Robinson Equation of State for calculation of heat capacity, (c) simple flow model with mass-averaged heat capacity. Symbols represent experimental points and lines model results. The location of temperature measurements in the reactor are: r = 13 mm and L = 0.2, 0.8, 1.2 and 1.4 m; and r = 33 mm and L = 0.23, 0.65, 1.1 and 1.4 m.

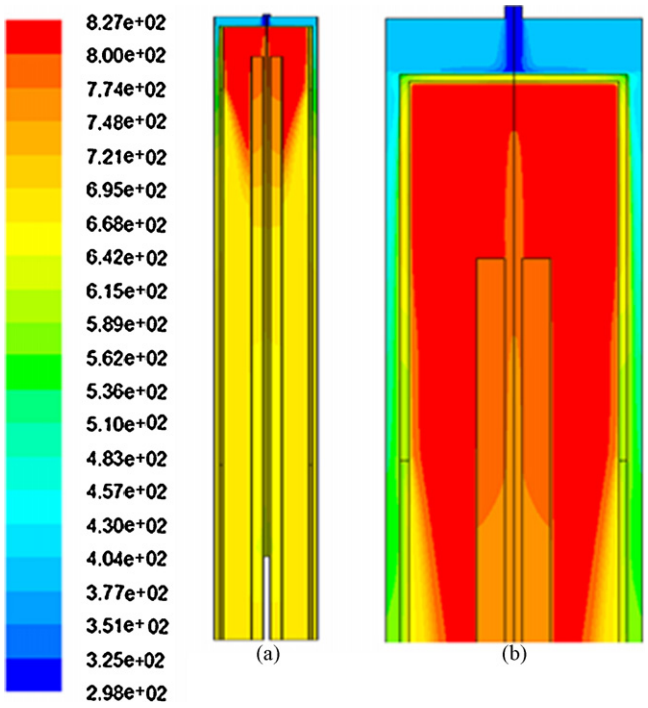

Fig. 4. Calculated temperature contours in the whole reactor (a). An enlargement of the upper section of the reactor is shown in the second temperature contour (b). The walls of the static mixer are located near the centre of the reactor, and the reaction chamber wall is located close to the external part of the reactor. The point in which the reaction chamber wall begins to be transpiring is marked with a black line.

positive deviations of calculated outlet temperature with respect to experimental data. The model correctly predicts the nearly flat temperature profiles that have been experimentally observed in the lower section of the reactor. The temperature of the transpiring flow is also well predicted.

Similar conclusions can be obtained by comparison of experimental and calculated temperature profiles with other process conditions. Such comparisons with several other process conditions are provided as Supplementary Material (Fig. S3).

4.2. Temperature, velocity and composition contours

In Fig. 4, temperature contours corresponding to a simulation performed considering the operating conditions described in Section 4.1 are presented. It can be seen that the highest temperatures are observed in the upper section of the reaction chamber, in the area in which the reaction chamber wall is not yet porous. In this section, calculated temperatures reach values above 800 K. In contrast, temperature in the upper section of the transpiring wall chamber remains low, at temperatures around 450 K. This temperature only starts to increase near the lateral, transpiring section of the wall. The transpiring flow is able to create a temperature gradient near the wall. This temperature gradient is particularly clear in the surroundings of the point in which the wall starts to be porous. After this point, the transpiring water flow into the reaction chamber rapidly quenches the reaction mixture, and a nearly constant temperature is observed in the rest of the reactor.

Temperature increase in the upper section of the reaction chamber is of course associated with the heat released by the oxidation. Fig. 5 presents the acetic acid composition contour in the reactor. It can be seen that in the static mixer, organic matter is only partially converted into acetic acid, the slow-oxidizing reaction intermediate according to the kinetic scheme used. The conversion to the reaction intermediate is completed only after the reaction mixture has entered into the reaction chamber. Due to the comparatively slow oxidation kinetics of acetic acid, a certain residence time is required for completely oxidizing it which is longer than the residence time inside the static mixer only. Because of this, high concentrations of acetic acid are observed in the upper section of the reaction chamber in Fig. 5. On the other hand, the concentration of acetic acid in the effluent is nearly zero, in agreement with the very high oxidation efficiencies observed in experiments with this reactor. On the other hand, this result supports the simplifications introduced in the model regarding the fluid mechanics in the static mixer: even if with these simplifications (i.e. considering feed and oxidant completely mixed already at the beginning of the static mixer) the in the static mixer obtained with the model must be higher than the conversion in real experiments, the progress of the reaction in the static mixer is small, and therefore the simplifications in the feed flow will have a small influence on final results.

Calculated path lines are presented in Fig. 6. Colour of lines in this figure indicates the residence time of fluid up to that point in the reactor. It can be seen that one of the most notable aspects of the fluid dynamics of the reactor is the existence of large recirculation areas in the upper part of the reaction chamber. Moreover, in this section of the reaction chamber, high flow velocities exist (up to 5 m/s), with high turbulent kinetic energies and turbulent kinetic energy dissipation rates (results not shown), demonstrating a strong influence of turbulent flow in fluid mixing in this section. These areas correspond to the section in which most of the oxidation reaction progress is occurring, as shown in Fig. 5. This result is in agreement with the results obtained with models based on simple flow patterns [16], which showed good agreement with experimental results when the upper part of the reactor was modelled as a completely stirred tank reactor (CSTR). Furthermore, this result indicates that although different flow patterns are observed in other parts of the reactor, the section in which reaction is taking place resembles a perfectly mixed CSTR reactor, which may have

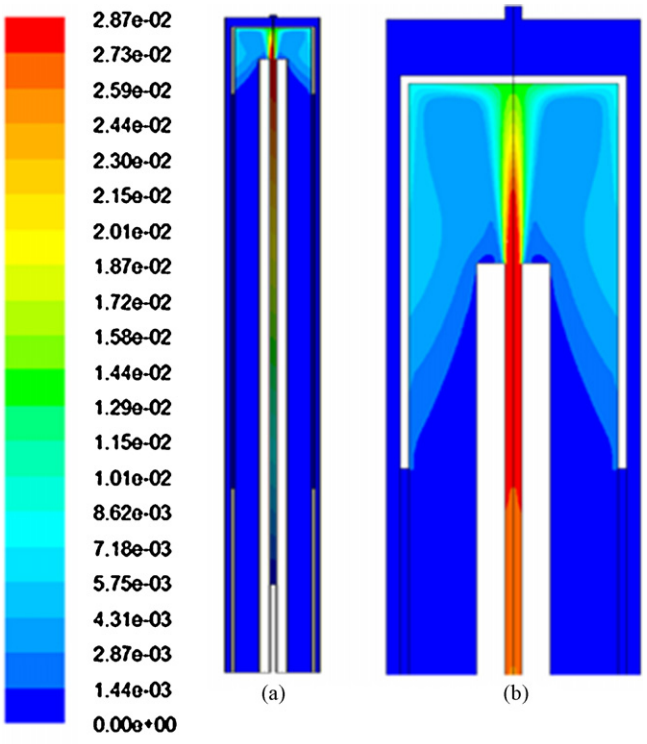

Fig. 5. Calculated acetic acid composition contours in the whole reactor (a). An enlargement of the upper part of the reactor is shown in the second contour (b).

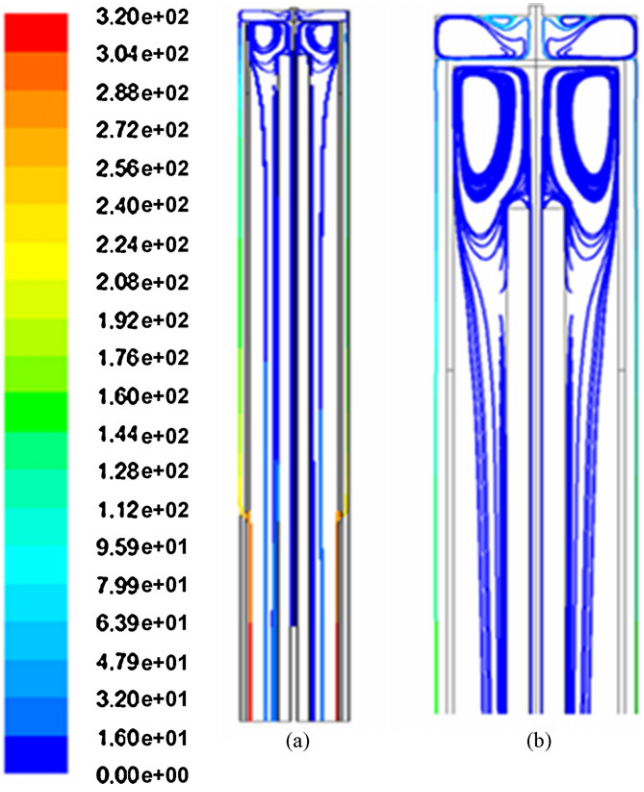

Fig. 6. Calculated path lines in the whole reactor (a). Lines are coloured by residence time. An enlargement of the upper part of the reactor is shown in the second contour (b).

implications concerning the reaction mechanisms in this reactor such as the occurrence of reactions with radicals. Calculated path lines also show that shortly after the beginning of the porous section of the reaction chamber wall, the reaction mixture is pushed to the centre of the reactor by the inflowing transpiring water. Therefore, it can be concluded that the transpiring water flow is accomplishing its function of protection of the transpiring wall. This figure also shows that the residence time of the feed entering through the static mixer is of about 60 s, while the residence time of transpiring flow can be as high as 320 s. In the lower part of the reaction chamber, fluid velocities are low (0.1–0.5 m/s) and turbulence has a smaller influence.

4.3. Analysis of the influence of process parameters

In this section, the influence of the main process parameters on temperature profiles in the reaction chamber is discussed. Unless otherwise specified, conditions used in simulations reported in this section are the same already described in Section 4.1.

One of the process parameters with a stronger effect on reactor performance is the transpiring flow ratio (TFR) [13]. This ratio is defined as the relationship between the flow rate of transpiring water and the flow rates of feed and oxidant, as it is shown in Eq. (2):

$$\mathrm{TFR} = \frac{\text{transpiring waterflow (kg h)}}{\text{feedflow (kg/h)} + \text{oxidantflow (kg/h)}} \quad (2)$$

Fig. 7 shows the calculated temperature contours in the upper part of the reaction chamber. Process conditions considered for the calculations of Fig. 7(b) are the same as in Sections 4.1 and 4.2, which correspond to TFR = 0.4. In Fig. 7(a), TFR has been reduced to 0.2, and in Fig. 7(c), it has been increased to 1.0. It can be seen that an increase of the TFR not only causes the apparition of steeper radial temperature profiles after the point in which the wall becomes porous, but also a reduction in the temperature of the upper, non-porous section of the reaction chamber, due to enhanced heat dissipation by conduction through the reaction chamber wall. An increase in the TFR also results in a considerable decrease of the temperature of the transpiring wall. Logically, with higher TFR, effluent temperature is lower as a consequence of the global energy balance. For this reactor design, it is advantageous to have sub-critical temperatures ($T < 647$ K) in the lower part of the reactor, so salts can flow out of the reaction chamber in an aqueous solution. According to model results TFR higher than 0.6 are required for this purpose. Experimental results indicate that lower TFR are suf-

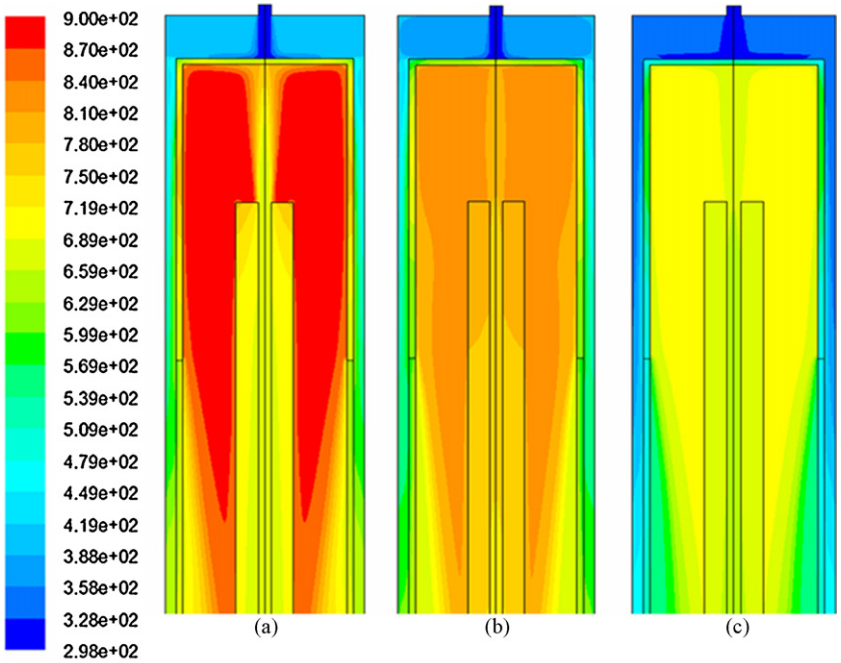

Fig. 7. Temperature contours in the upper part of the reactor for different values of the transpiring flow ratio (TFR): (a) TFR = 0.2; (b) TFR = 0.4; (c) TFR = 1.0.

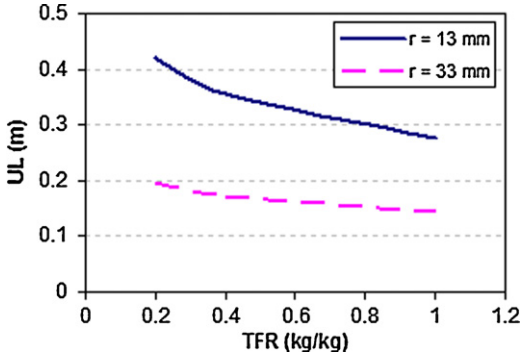

Fig. 8. Variation of reactor Useful Length (UL) with the transpiring flow ratio (TFR).

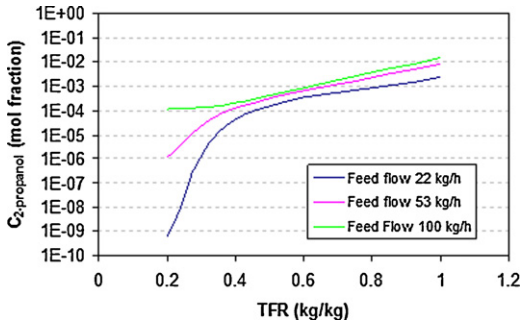

Fig. 10. Variation of the concentration of acetic acid in the effluent as a function of feed flow rate and TFR (ordinate axis logarithmically scaled).

ficient [13]. This discrepancy is a consequence of the overprediction of reactor outlet temperatures as a consequence of not considering heat losses to the environment, as already discussed in Section 4.2.

Another important consequence of an increase of TFR is a reduction of the volume of the reactor in which temperature is sufficiently high for continuation of the oxidation reaction, defined as the Useful Length (UL) in a previous work [13]. In this work, the UL has been defined as the length in which temperature is above 740 K, which approximately is the autoignition temperature of 2-propanol in water [31]. Fig. 8 shows the variation of UL with TFR at two different radial positions. UL between 0.2 and 0.4 m are obtained, and it is observed that UL decreases when TFR increases, in agreement with experimental results [13].

As already described in Section 1, the reactor has operated both in a pilot plant designed for a maximum feed flow of 40 kg/h and in a bigger plant for a feed flow of 200 kg/h. Therefore a study of the differences in the performance of the reactor when feed flow is increased within this range has been carried out. Fig. 9 also presents temperature contours in the upper part of the reactor corresponding to different values of TFR (0.2, 0.4 and 1.0), but with a higher feed flow rate of 100 kg/h compared to the flow rate of 22 kg/h considered in the previous simulations. As in the simulations performed with a lower flow rate presented in Fig. 7, Fig. 9 shows that an increase in TFR results in steeper radial temperature profiles as well as a global reduction in the temperature in the upper, non-porous section of the reaction chamber. However, comparison of Figs. 7 and 9 shows that higher temperatures are achieved in the reaction chamber if feed flow rate is increased even if the same TFR is maintained. This can be explained by the fact that the amount of heat released by the reaction increases when the feed flow is increased, while the surface available for heat dissipation is constant. Moreover, by comparing Figs. 7 and 9 it can be seen that the temperature of the transpiring wall is lower when the feed flow is increased with a constant TFR.

A further effect of increasing the feed flow rate is shown in Fig. 10. This figure presents the variation of acetic acid concentration in the effluent as a function of feed flow and TFR. Very low concentrations are obtained with most operating conditions, demonstrating the high efficiency of the process. The exception is the results with TFR = 1.0, which shows a certain acetic acid concentration which increases when the feed flow rate is increased. This result demonstrates that when flow rate is increased, lower TFR are required in order to achieve high waste destruction efficiency. With a lower TFR, a higher temperature is reached in the reaction chamber which compensates the reduction in the residence time

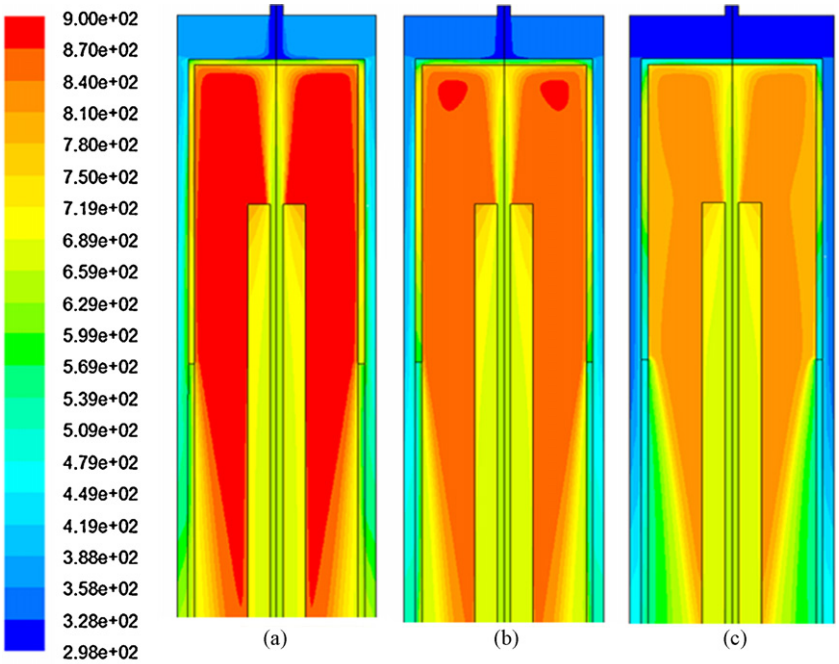

Fig. 9. Temperature contours in the upper part of the reactor for different values of the transpiring flow ratio (TFR) with feed flow rate of 100 kg/h: (a) TFR = 0.2; (b) TFR = 0.4; (c) TFR = 1.0.

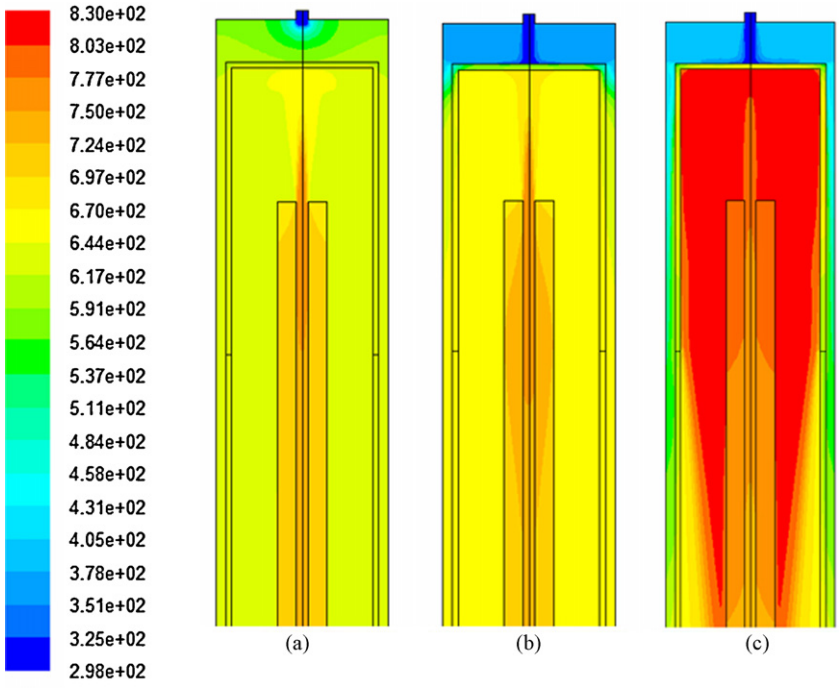

Fig. 11. Temperature contours: (a) transpiring wall design 1, all the transpiring wall is porous; (b) transpiring wall design 2, the upper cup of the transpiring wall is not porous; (c) transpiring wall design 3, the upper cup and the upper section of the cylindrical element of the transpiring wall are not porous.

in the reactor caused by the increase in flow rates. The combination of this result with the previous observation that indicated that lower TFRs were required to cool the transpiring wall down to the same temperature when feed flow rate is increased, allows concluding that for operation at high flow rates, lower TFRs than those required with low flow rates are adequate. On the other hand, for achieving the sub-critical temperatures in the effluent required for dissolving the salts, a constant TFR is required as indicated by the global energy balance. Therefore, for operation of this reactor with high flow rates, the injection of a second stream of cool water in the lower part of the reactor would be appropriate. With this solution, it would be possible to operate the reactor with a relatively low TFR in order to protect the wall and to allow reaching sufficiently high temperatures in the reaction chamber, and at the same time to cool the effluent down to sub-critical temperatures with the second water stream.

The SCWO can also be carried out using pure oxygen as oxidant instead of air. Simulation results (shown in Fig. S4 of Supplementary Information) demonstrate that if oxygen is used, a smaller reactor volume and therefore a shorter residence time is required for completely oxidizing the acetic acid. The reason for this is that nitrogen in air acts as a diluent and a temperature buffer. Therefore when pure oxygen is used, higher temperatures (with a maximum temperature of 930 K in the case of operation with oxygen, compared to 870 K when air is used) and higher reaction rates can be achieved. Therefore it is possible to increase the treatment capacity of the reactor by using oxygen instead of air as oxidant.

The model has also been used to analyse the effect of the transpiring flow inlet temperature, which is another important process parameter. Three inlet temperatures have been tested: 298, 473 and 673 K. The variations observed in the flow path lines are minimal (shown in Fig. S5 of Supplementary Information). Therefore, a transpiring water flow with a high inlet temperature has equivalent capacity for protecting the transpiring wall as a colder flow with respect to the separation of the flow lines from the wall. On the other hand, if the inlet temperature of the transpiring flow is increased, temperature in the reaction chamber is decreased to a lower extent by heat transfer. Therefore, if the temperature of the transpiring water is increased, it is possible to operate the reactor with higher transpiring flow rates without quenching the reaction. The maximum allowable temperature of transpiring water is limited by the resistance of the porous material to high temperatures, which in the case of the Ni-alloy used in the reactor of the University of Valladolid is 873 K.

4.4. Comparison of different transpiring wall designs

As described in Section 2, three different transpiring wall designs have been tested with this reactor. Fig. 11 shows a comparison of temperature contours in the upper section of the reaction chamber. Process conditions considered in these simulations are the same described in Section 4.1. In comparison with the temperature contours obtained with transpiring wall design 3 (according to the nomenclature used in Fig. 1), it can be seen that both with designs 1 and 2, lower temperatures are observed in the upper part of the reaction chamber (with a maximum temperature of 760 K with design 1 and 770 K with design 2, compared to 830 K with design 3). The reason for this is that with designs 1 and 2 the transpiring flow is already flowing into the reaction chamber in the upper section and therefore the reaction mixture is cooled down to a higher extent. Because the reaction mixture is cooled down more rapidly with transpiring wall designs 1 and 2, it can be concluded that these designs are less appropriate for diluted feeds, because the oxidation would be quenched before being completed, but they are more appropriate for very concentrated feeds because they allow a better control of maximum reaction temperatures.

Another feature that can be observed in Fig. 11 is that the temperature of the upper part of the transpiring wall is very similar with all three designs (600–620 K). On the other hand, Fig. 12 shows the flow path lines in the upper section of the reactor with the three transpiring wall designs. It can be seen that when the lateral section of the wall is transpiring in all its length, as with designs 1 and 2, the reaction mixture is effectively pushed away from the transpiring wall already in the upper part of the reaction chamber.

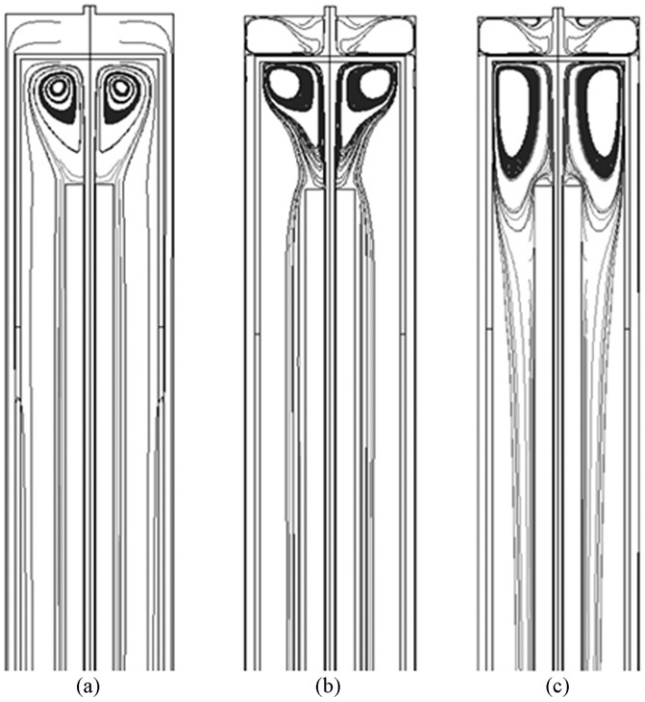

Fig. 12. Flow path lines: (a) transpiring wall design 1, all the transpiring wall is porous; (b) transpiring wall design 2, the upper cup of the transpiring wall is not porous; (c) transpiring wall design 3, the upper cup and the upper section of the cylindrical element of the transpiring wall are not porous.

In contrast, comparing the path lines obtained with designs 1 and 2, it can be seen that the flow pattern in the upper section of the reaction chamber is almost identical regardless if the upper cup of the wall is transpiring or not: the reaction mixture flows out of the mixer at relatively high velocities (approximately 5 m/s) and flows up until it collides with the upper cup of he wall. The transpiring flow, on the other hand, flows into the reaction chamber at low velocities (approximately 0.005 m/s) because it is homogeneously distributed along the entire transpiring wall, and it is unable to push the reaction mixture leaving the mixer away from the upper cup. For this reason, the upper cup of the transpiring wall can be subjected to harsher conditions and sustain more damage due to high temperatures and corrosion than the remaining parts of the reactor. Indeed, it has been experimentally observed that the upper cup of the reaction chamber suffered more damage during operation than other parts of the transpiring wall [13]. Because sinterized, porous metal is less corrosion resistant than normal metal sheets it is recommendable to use non-porous metal sheets for construction of the upper cap of the transpiring wall, as in designs 2 and 3.

5. Conclusions

A computational fluid dynamic (CFD) model of a transpiring wall supercritical water oxidation reactor has been presented. The model has been validated by comparison with experimental results, and the influence of different process conditions as well as of the design of the transpiring wall has been analysed.

It has been observed that the main limitations of the model are the calculation of the fluid mixture heat capacity as a mass average of pure component heat capacities, as imposed by the restrictions of the code used for simulations, and the simplifications regarding the flow in the static mixer, which has been considered monophasic although in reality a biphasic gas–liquid flow exists until the reaction mixture is heated up to supercritical temperatures. Due to these simplifications, the model underpredicts maximum reaction temperatures by approximately 100–150 K depending on process conditions. Reactor outlet temperatures and effluent compositions are well predicted by the model, with maximum deviations of 50 K.

In agreement with experimental results, simulations show that the transpiring water flow ratio (Eq. (2)) is one of the main process parameters that allow controlling the maximum reaction temperature as well as effluent temperature, which has to be sub-critical to ensure that salts are dissolved in the effluent in order to avoid clogging of down-flow lines. If feed flow is increased, a lower transpiring water flow ratio is required to reduce the maximum reaction temperature and transpiring wall temperatures to the same extent. It has been shown that reactor capacity can be increased by using pure oxygen instead of air as oxidant.

The behaviour of different transpiring wall designs has been tested. It has been shown that reaction chamber walls with a non-transpiring section are more appropriate to treat diluted feeds, because they allow reaching higher reaction temperatures before the oxidation is quenched by transpiring water. On the contrary, a completely transpiring wall is more adequate for controlling maximum reaction temperatures with more concentrated feeds. It has been shown that the upper part of the reaction chamber sustains the harsher conditions due to the contact with the hot reaction mixture leaving the static mixer. The use of a transpiring, porous material in this section of the reaction chamber has a very small impact on the flow pattern in the reaction chamber, and therefore it is recommendable to use a more durable, non-porous metal sheet for construction of this part of the reactor instead of a porous material.

Acknowledgements

Partially financed by the Spanish Ministry of Science and Innovation project, PET 2006-0376. M.D. Bermejo thanks the Juan de la Cierva program (JCI-2008-02877) funded by the Ministerio de Ciencia e Innovación (Spain). A. Martín thanks the Alexander von Humboldt foundation (Germany) for a postdoctoral research fellowship.

Appendix A. Supplementary data

Supplementary data associated with this article can be found, in the online version, at doi:10.1016/j.cej.2010.01.013.

References

[1] M.D. Bermejo, M.J. Cocero, Supercritical water oxidation: a technical review, AIChE J. 52 (11) (2006) 3933–3951.
[2] G. Brunner, Near and supercritical water. Part II. Oxidative processes, J. Supercrit. Fluids 47 (2009) 382–390.
[3] P.A. Marrone, M. Hodes, K.A. Smith, J.W. Tester, Salt precipitation and scale control in supercritical water oxidation. Part b. Commercial/full-scale applications, J. Supercrit. Fluids 29 (2004) 289–312.
[4] P. Kritzer, E. Dinjus, An assessment of supercritical water oxidation (SCWO). Existing problems, possible solutions and new reactor concepts, Chem. Eng. J. 83 (2001) 207–214.
[5] M.D. Bermejo, D. Rincon, A. Martín, M.J. Cocero, Experimental performance and modeling of a new cooled wall reactor for the supercritical water oxidation, Ind. Eng. Chem. Res. 48 (13) (2009) 6262–6272.
[6] Y. Calzavara, C. Joussot-Dubien, H.A. Turc, E. Fauvel, S.A. Sarrade, A new reactor concept for hydrothermal oxidation, J. Supercrit. Fluids 31 (2004) 195–206.
[7] M.D. Bermejo, F. Cantero, M.J. Cocero, Supercritical water oxidation of feeds with high ammonia concentrations: pilot plant experimental results and modelling, Chem. Eng. J. 137 (2008) 542–549.
[8] S. Baur, H. Schmidt, A. Krämer, J. Gerber, The destruction of industrial aqueous waste containing biocides in supercritical water—development of the SUWOX process for the technical application, J. Supercrit. Fluids 33 (2005) 149–157.
[9] B. Veriansyah, J.-D. Kim, J.-C. Lee, A double wall reactor for supercritical water oxidation: Experimental results on corrosive sulfur mustard simulant oxidation, J. Ind. Eng. Chem. 15 (2009) 153–156.
[10] E. Fauvel, C. Joussot-Dubien, P. Guichardon, G. Charbit, F. Charbit, S. Sarrade, A double-wall reactor for hydrothermal oxidation with supercritical water flow across the inner porous tube, J. Supercrit. Fluids 28 (2004) 47–56.

[11] J. Abeln, M. Kluth, M. Böttcher, W. Sengpiel, Supercritical water oxidation (SCWO) using a transpiring wall reactor: CFD simulations and experimental results of ethanol oxidation, Environ. Eng. Sci. 21 (2004) 93–99.
[12] B. Wellig, K. Lieball, P. Rudolph Von Rohr, Operating characteristics of a transpiring-wall SCWO reactor with a hydrothermal flame as internal heat source, J. Supercrit. Fluids 34 (2005) 35–50.
[13] M.D. Bermejo, F.F. Polanco, M.J. Cocero, Effect of the transpiring wall on the behavior of a supercritical water oxidation reactor: modeling and experimental results, Ind. Eng. Chem. Res. 45 (2006) 3438–3446.
[14] M.D. Bermejo, M.J. Cocero, Destruction of an industrial wastewater by supercritical water oxidation in a transpiring wall reactor, J. Hazard. Mater. 137 (2) (2006) 965–971.
[15] E. Fauvel, C. Joussot-Dubien, E. Pomier, P. Guichardon, G. Charbit, F. Charbit, S. Sarrade, Modeling of a porous reactor for supercritical water oxidation by a residence time distribution study, Ind. Eng. Chem. Res. 42 (2003) 2122–2130.
[16] M.D. Bermejo, F.F. Polanco, M.J. Cocero, Modeling of a transpiring wall reactor for the supercritical water oxidation using simple flow patterns: comparison to experimental results, Ind. Eng. Chem. Res. 44 (11) (2005) 3835–3845.
[17] C.H. Oh, R.J. Kochan, T.R. Charlton, A.L. Bourhis, Thermal-hydraulic modeling of supercritical water oxidation of ethanol, Energy Fuels 10 (1996) 326–332.
[18] N. Zhou, A. Krishnan, F. Vogel, W.A. Peters, A computational model for supercritical water oxidation of organic toxic wastes, Adv. Environ. Res. 4 (2000) 79–95.
[19] S. Moussière, C. Joussot-Dubien, P. Guichardon, O. Boutin, H.-A. Turc, A. Roubaud, B. Fournel, Modelling of heat transfer and hydrodynamic with two kinetic approaches during supercritical water oxidation process, J. Supercrit. Fluids 43 (2007) 324–332.
[20] J. Sierra-Pallares, M.T. Parra-Santos, J. García-Serna, F. Castro, M.J. Cocero, Numerical modelling of hydrothermal flames. Micromixing effects over turbulent reaction rates, J. Supercrit. Fluids 50 (2) (2009) 146–154.
[21] C. Narayanan, C. Frouzakis, K. Boulouchos, K. Príkopský, B. Wellig, P. Rudolf von Rohr, Numerical modelling of a supercritical water oxidation reactor containing a hydrothermal flame, J. Supercrit. Fluids 46 (2008) 149–155.
[22] M.D. Bermejo, D. Rincón, V. Vázquez, M.J. Cocero, Supercritical water oxidation: fundamentals and reactor modeling, CI&CEQ 13 (2) (2007) 79–87.
[23] J. Sierra-Pallares, M.T. Parra-Santos, J. García-Serna, F. Castro, M.J. Cocero, Numerical analysis of high-pressure fluid jets: application to RTD prediction in supercritical reactors, J. Supercrit. Fluids 49 (2009) 249–255.
[24] L. Li, P. Chen, E.F. Gloyna, Generalized kinetic model for wet oxidation of organic compounds, AIChE J. 37 (11) (1991) 1687–1697.
[25] M.J. Cocero, J.L. Martínez, Cool wall reactor for supercritical water oxidation: modeling and operation results, J. Supercrit. Fluids 31 (2004) 41–55.
[26] P.J. Linstrom, W.G. Mallard (Eds.), NIST Chemistry WebBook, NIST Standard National Institute of Standards and Technology, Gaithersburg MD, 20899. http://webbook.nist.gov.
[27] C. Magoulas, D. Tassios, Thermophysical properties of n-alkanes from C_1 to C_{20} and their prediction for higher ones, Fluid Phase Equilibr. 56 (1990) 119–140.
[28] M.D. Bermejo, A. Martín, M.J. Cocero, Application of the Anderko–Pitzer EoS to the calculation of thermodynamic properties of systems involved in the supercritical water oxidation process, J. Supercrit. Fluids 42 (1) (2007) 27–35.
[29] R.J. Kochan, C.H. Oh, CFD Model Development and Data Comparison for Thermal-Hydraulic Analysis of HTO Pilot Scale Reactor, Idaho National Engineering Laboratory, 1995.
[30] M.D. Bermejo, P. Cabeza, M. Bahr, R. Fernández, V. Ríos, C. Jiménez, M.J. Cocero, Experimental study of hydrothermal flames initiation using different static mixer configurations, J. Supercrit. Fluids 50 (3) (2009) 240–249.
[31] R.M. Serikawa, T. Usui, T. Nishimura, H. Sato, S. Hamada, H. Sekino, Hydrothermal flames in supercritical water oxidation: investigation in a pilot scale continuous reactor, Fuel 81 (2002) 1147–1159.